A Novel Strategy for the Surface Current Determination From Marine X-Band Radar Data

Francesco Serafino, Claudio Lugni, and Francesco Soldovieri

***Abstract*—This letter deals with the sea state monitoring starting from marine radar images in the X-band. For such a topic, one of the key factors affecting the reliability of reconstruction procedure is the determination of the equivalent surface current that also accounts for the velocity of a moving ship. In this letter, we propose a method to evaluate the surface current, particularly for large values. The reliability of the proposed procedure is shown by a numerical analysis with synthetic data. Subsequently, we present some preliminary results with experimental data collected by a radar on a moving ship.**

***Index Terms*—Image sequence analysis, marine radar, sea current, sea state.**

I. Introduction

THE MONITORING of sea state starting from marine radar images is of timely interest, since radar systems give the opportunity to scan the sea surface with high temporal and spatial resolution [1]–[6]. This possibility arises due to the fact that the backscattering from the sea is "visible" on the marine radar images (ranging to some kilometers from the observation platform) under some conditions [5]. These radar signatures are considered as clutter when the radar is exploited for the usual aim of navigation control. Differently, these signatures represent the "useful signal" to be processed when the aim is to achieve a spatial–temporal image of the sea state.

The backscattering by the sea arises due to the presence on the sea surface of the capillary waves (ripples) caused by the action of the wind. In particular, the longer waves modulate the backscattering phenomenon, and thus, they become visible in the "radar" images. More in details, such a modulation arises due to three effects: hydrodynamic modulation (HM), tilt modulation (TM), and shadowing (SH). HM describes the modulation of the energy of the ripples induced by the interaction with the longer waves, TM is the modulation due to the variation of the angle under which the ocean wave is viewed by the radar, and SH accounts for the electromagnetic shadowing of the sea surface by higher waves [7]–[9].

As a result, the radar image is not a direct representation of the sea state, and thus, a transformation procedure is needed. In particular, the data processing is cast as an inversion problem where, starting from the time series of spatial radar imagery collected at different time instants, one aims at determining the elevation $\eta(x, y, t)$ of the sea surface meant as a function of two spatial variables (related to the zone investigated by the radar) and of the time. The inversion scheme here considered is linear and can be summarized as follows [3]. After a Fourier transform of time–space data, a spectral filter is used to erase all the undesired phenomenon via a dispersion relation. The use of modulation transfer function (MTF) allows the transformation from the radar spectrum to sea spectrum; finally, the resulting spectrum is Fourier inverse transformed to return to the space–time domain. The two intermediate steps affect the reliability of the inversion procedure. MTF determination has been the subject of significant activity based on experimental/numerical analyses, and some assessed conclusions on this point have been reached [3].

Here, we focus to the problem of the determination of the dispersion relation exploited to filter out the undesired phenomena [3], [4]. In fact, when the surface currents are not correctly determined and/or accounted for in the dispersion relation, the filtering is incorrect, and thus, the results of the overall inversion become quite poor. This drawback is further increased for high values of the surface current since the problem of the determination of the current becomes quite complicated, and particular care has to be made to the filtering procedure.

In this letter, we will present a new strategy to determine the equivalent surface current meant as the sum of the (possible) relative motion of the radar platform (ship) with respect to the ocean and of the actual ocean current. The proposed strategy is based on the "correlation" between the measured spectrum and the characteristic function defined on a support coinciding with the dispersion relation (evaluated as a function of the unknown surface current components). The reliability of this strategy is first tested against synthetic data, and a comparison with the standard least squares (LS) fitting method [1], [3] is also presented. Then, we present an application of the proposed strategy to the case of experimental data collected by a radar antenna installed on a ship whose speed is accurately measured through a GPS system mounted onboard.

II. Data Processing Approach

This session is devoted to briefly describe the reconstruction procedure to extract the sea state parameters from radar data, in terms of direction, wavelength, period, and significant and maximum wave height, and to monitor the temporal–spatial behavior of surface elevation.

Manuscript received February 11, 2009; revised April 12, 2009 and June 24, 2009. Date of publication October 30, 2009; date of current version April 14, 2010.

F. Serafino and F. Soldovieri are with the Institute for Electromagnetic Sensing of the Environment, National Research Council, 80124 Napoli, Italy (e-mail: soldovieri.f@irea.cnr.it).

C. Lugni is with the Department of Seakeeping and Maneuverability, The Italian Ship Model Basin (INSEAN), 00128 Roma, Italy (e-mail: c.lugni@linsean.it).

Color versions of one or more of the figures in this paper are available online at http://ieeexplore.ieee.org.

Digital Object Identifier 10.1109/LGRS.2009.2031878

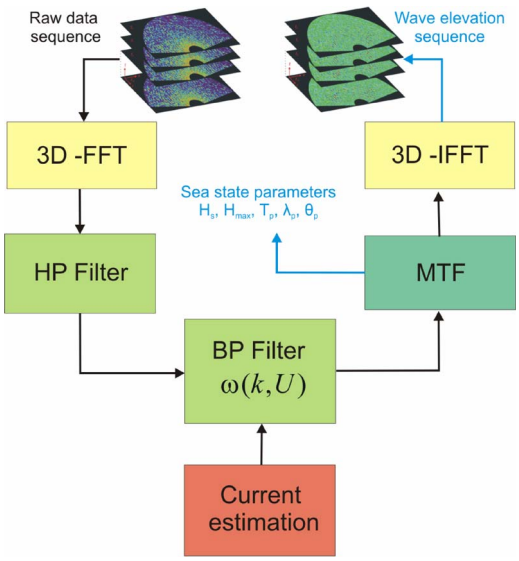

Fig. 1. Block diagram of the inversion procedure.

The algorithm is summarized in the block diagram of Fig. 1, where each block is detailed as follows. In the first step, the raw data image sequence is transformed into a 3-D image spectrum by means of a 3-D fast Fourier transform. To eliminate the effects due to the received signal power decay along the range, a high-pass (HP) filter is applied to the image spectrum $F(k_x, k_y, \omega)$ [3].

The second step aims to extract the linear gravity wave components from the HP filtered image spectrum $F_I(k_x, k_y, \omega)$. To this end, we exploit the dispersion relation that relates the wavenumber $\overline{k}$ to the angular frequency $\omega(\overline{k})$ and the current of the ocean surface $U = (U_x, U_y)$ as

$$\omega(\overline{k}) = \sqrt{gk\tanh(kh)} + \overline{k}\cdot\overline{U} \tag{1}$$

where g is the acceleration due to the gravity at the Earth's surface, $k = |\overline{k}| = \sqrt{k_x^2 + k_y^2}$, and h is the water depth.

The current vector $\widetilde{U} = (\widetilde{U}_x, \widetilde{U}_y)$ needs to be estimated before applying the dispersion relation [1]. This represents the key step of the full inversion procedure, since a bad estimate of the current translates into an incorrect filtering of the wave components. This crucial point is the main topic of this letter, and a novel strategy to face this task is presented in the following section.

Once the current $\widetilde{U} = (\widetilde{U}_x, \widetilde{U}_y)$ has been estimated, it is possible to build the bandpass filter $G(k_x, k_y, \omega, \widetilde{U}_x, \widetilde{U}_y)$ on the basis of (1) and apply it to the image spectrum $F_I(k_x, k_y, \omega)$ (see block diagram of Fig. 1). The result of this procedure is the function $\widetilde{F}_I(k_x, k_y, \omega)$. The next step is to move from the filtered image spectrum $\widetilde{F}_I(k_x, k_y, \omega)$ to the desired sea-wave spectrum $F_W(k_x, k_y, \omega)$ by minimizing the effect due to the modulation phenomena [8]. This step may be implemented by using the MTF [3]

$$F_W(k_x, k_y, \omega) = \frac{\widetilde{F}_I(k_x, k_y, \omega)}{|M(k)|^2} \tag{2}$$

where $|M(k)|^2 = k^\beta$ is the MTF. An empirical analysis provided that, in most cases, a good estimation is $\beta = -1.2$ [3]. When the wave spectrum $F_W(k_x, k_y, \omega)$ is determined, it is possible to extract some parameters about the sea state. This is performed by generating a wavenumber directional spectrum, whose maximum provides wavelength and propagation direction $[\lambda_p, \vartheta_p]$ of the primary wave. The last step provides the evolution of the wave height $\eta(x, y, t)$ by performing an inverse 3-D FFT to the function $F_W(k_x, k_y, \omega)$.

III. Surface Current Determination

This section deals with the problem of the surface current vector $\widetilde{U} = (\widetilde{U}_x, \widetilde{U}_y)$ that is a crucial step in ensuring the reliability of the overall data processing presented before.

If no external information about the current is available, such a quantity has to be estimated from the data.

The classical procedure [1], [5] is based on LS fitting to globally minimize the following functional:

$$Q(U_x, U_y) = \sum_i \sum_j \left[\omega(k_{xi}, k_{yj}) - \widetilde{\omega}(k_{xi}, k_{yj})\right]^2 \tag{3}$$

where $\omega(k_{xi}, k_{yj})$ denotes the frequencies associated to the model of (1), and $\widetilde{\omega}(k_{xi}, k_{yj})$ denotes the frequencies selected from the data where the energy of the amplitude of the spectrum $F_I(k_x, k_y, \omega)$ is larger than a fixed threshold [10].

Here, we propose a different technique that allows a more accurate estimation of the surface current. This method is based on the maximization of the normalized scalar product (NSP) between the amplitude of the filtered image spectrum $|F_I(k_x, k_y, \omega)|$ and the characteristic function $G(k_x, k_y, \omega, U_x, U_y)$ defined as

$$G(\overline{k}, \omega, \overline{U}) = \begin{cases} 1, & \text{if } \left|\sqrt{gk\tanh(kh)} + \overline{k}\cdot\overline{U} - \omega(\overline{k})\right| \le \Delta\omega/2 \\ 0, & \text{otherwise} \end{cases} \tag{4}$$

where $\Delta\omega$ is the frequency step used to sample the spectra.

The NSP (as function of the unknown current components U_x, U_y) is defined as

$$V(U_x, U_y) = \frac{\langle |F_I(k_x, k_y, \omega)|, G(k_x, k_y, \omega, U_x, U_y)\rangle}{\sqrt{P_F \cdot P_G}} \tag{5}$$

where P_F and P_G are the power associated to the image spectrum $|F_I(\cdot)|$ and $G(\cdot)$, respectively. The reliability of the proposed approach will be tested in the two following sections against synthetic and experimental data.

IV. Validation of the Approach by Synthetic Data

This section has a twofold aim of testing the validity of the proposed strategy against synthetic data and presenting a comparison with LS method.

A fully 2-D numerical wave maker [11] has been exploited to reproduce the physical conditions existing in a real wave tank (see Fig. 2). The spatial and time evolution of a free-surface $\partial\Omega_{\mathrm{SL}}$ wave train, generated through a hinged paddle $\partial\Omega_c$ moving with angular velocity $\dot{\alpha}(t)$, has been investigated by an inviscid model. In this framework, the mathematical statement

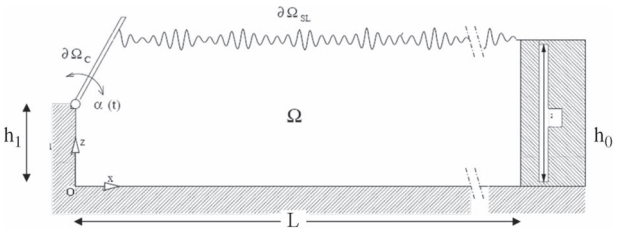

Fig. 2. Pictorial sketch of the mathematical problem. The geometrical parameters $h_0 = 3.6$ m, $h_1 = 1.8$, and $L = 230$ m.

is described through the Laplace equation for the velocity potential function. Once the velocity potential is computed on the boundary domain, the nonlinear free-surface equations are stepped forward by a fourth-order Runge–Kutta scheme, and the motion of the wave maker is updated.

To save computational time and memory for the simulation of long-time wave evolution, a domain decomposition technique has been used [12]. Further details of the numerical model used, as well as of the treatment of the free surface, can be found in [11].

A JONSWAP sea spectrum with $H_{1/3} = 0.094$ m and $T_0 = 1.97$ s has been reproduced in the numerical wave tank for the present case. A factor scale of 20 has been used to reconstruct the wave elevations corresponding to the full-scale sea state ($H_{1/3} = 1.88$ m and $T_0 = 8.8$ s). Here, $H_{1/3}$ represents the significant wave height, and T_0 is the modal period associated with the prescribed spectrum.

An average wave spectrum was computed from three independent simulations of the wave field with a duration of 6 min; the data are sampled with a time step of 0.34 s and a spatial step of 0.6 m. In particular, we have $Nx = 6306$ spatial samples, leading to an extent of 3750 m, and $Nt = 1066$ time samples, leading to an overall acquisition time of 6 min.

The averaged data have been decimated, so that the samples actually used to perform the reconstruction are $Nx = 630$ and $Nt = 32$ with steps of 5.9 m and 2.4 s; this leads to spatial and time extent of 3717 m and 76.8 s (in model scale), respectively. The effects of surface current were added for 17 different values of current ranging from 0 to -10 m/s.

For each of the 17 data sets relative to the ocean surface current values, the corresponding radar data have been simulated using the procedure proposed in [3]. Starting from each radar image set, the ocean current has been evaluated via the NSP procedure presented in the previous section and the classical LS method.

Fig. 3 shows the comparison between the performances of the NSP and LS methods. As it can be seen, the LS method performances deteriorate as long as the value of the ocean current increases, while the NSP method is able to determine the right value of the current even for large values of it.

The residual error of the estimation of the current by NSP is shown in Fig. 4. We can appreciate the good performances of the NSP procedure that is able to estimate the ocean surface current with a residual error having a standard deviation of 0.05 m/s.

The better performances of the NSP-based method compared to the LS one can be briefly justified. As said previously, the LS method is based on two steps: the first one is the determination

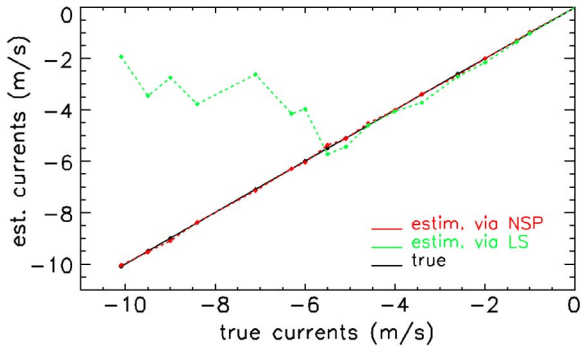

Fig. 3. Comparison between the negative current values. (Solid line) True. (Green) Reconstructed via the LS method. (Red line) Reconstructed by the NSP method.

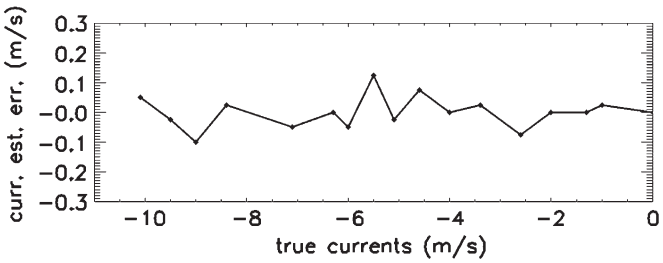

Fig. 4. Residual error on the current values retrieved by NSP.

of the "measured locus of points," where the spectrum is significant (by a thresholding procedure); in the second step, the global minimum of the cost function in (3) is attained. Thus, since a threshold procedure is exploited, particularly at lower levels of the measured spectrum, noise plays a relevant role and can be decisive in establishing if a point has to be considered or not in the retained locus of points. In addition, when such a point has been considered reliable, it plays in the minimization of (3) the same role as the other ones associated to the more significant levels of the spectrum; it is evident that all the aforementioned factors can badly affect the current determination procedure.

Differently, in the NSP-based method, we have the lower levels of the spectrum, which play a weaker role compared to the significant ones in the determination of $V(U_x, U_y)$ [see (5)], thus improving the reliability of the estimate.

It is worth noting that the different performances between the two methods arise because of the spectra aliasing influencing the data for larger values of the surface current. As a general comment, an accurate knowledge, not ever available, of the total advecting current (given as the sum of the ship velocity and the surface current) is needed to compensate the aliasing effects. Here, we show how the NSP method allows accurately estimating the total advecting current also when we do not exploit any *a priori* information about the ship velocity. The situation is quite different for the LS method, whose performances can be seen to break down at stronger currents, where temporal aliasing causes incorrect estimation of the frequencies of the dominant spectral peaks. Differently, the NSP method, which uses the entire spectrum, does not break down because the characteristic function G filters out all aliased information.

A further statement of the different performances of the two methods can be inferred by Fig. 5, showing the comparison

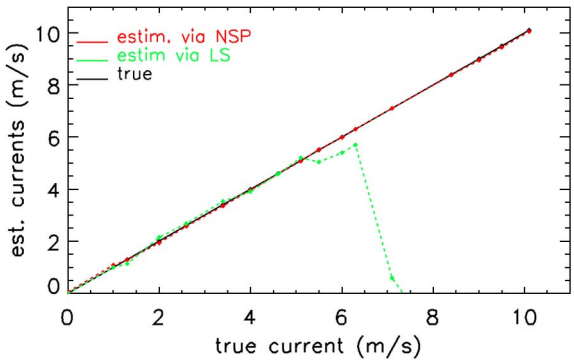

Fig. 5. Comparison between the positive current values. (Solid line) True. (Green) Reconstructed via the LS method. (Red line) Reconstructed by the NSP method.

in the case of opposite total advecting current. In this case, we have NSP performances that are very similar to the ones achieved when negative values of the current are considered (see Fig. 3) and that remain remarkably better that the ones achieved by LS method.

V. Application to the Full-Scale Experimental Case

This section is devoted to present some preliminary experimental results about the determination of the surface current via the NSP procedure.

The raw data are recorded by a radar FURUNO FAR2117 installed on a moving ship and consist of a sequence of 32 images, each one made up of 600 × 600 pixels; the azimuth and range resolutions are equal to 4.6 m, so that the total area of each image is about 8 km^2. The time sampling is 2.4 s, so that a complete time acquisition of about 76.8 s is achieved. The spatial and temporal radar parameters lead to spectral resolution parameters of $\delta k_x = \delta k_y = 2.27 \times 10^{-3}$ rad/m and $\Delta\omega = 8.01 \times 10^{-2}$ rad/s. In particular, we are concerned with the processing of a data set recorded on November 22, 2007 in the area of the Mediterranean sea between Malta and Sicily islands. For such a data set, the known ship speed ν_{ship} varies around a value of about 8 m/s; such a speed was measured by a GPS instrument properly installed onboard. Since the radar measures the sea spectrum in a reference system fixed with the ship, the total current vector U in (1) is given as $U = V_{\text{ship}} + U_{\text{sc}}$, i.e., the ship "feels" (or "sees") a current which is the sum of the ship speed and the surface current. Since V_{ship} is measured through a GPS system, the proposed approach allows for a proper estimation of the surface current U_{sc}. By taking in mind this difference, in the following, we will distinguish between the total current component U and the surface current U_{sc}.

The NSP procedure has been tested for such a data set corresponding to 105 min of acquisition. Fig. 6 shows the result of the comparison between (black line) the current component U_y along the ship motion and (red line) the GPS recording of the ship speed. Fig. 7 shows the intensity $\sqrt{U_x^2 + (U_y - V_{\text{ship}})^2}$ (panel A) and the direction with respect to north (panel B) of the estimated residual ocean current after the removal of the ship velocity.

These results, obtained in an independent way by the GPS instruments and by the NSP algorithm, show a satisfactory

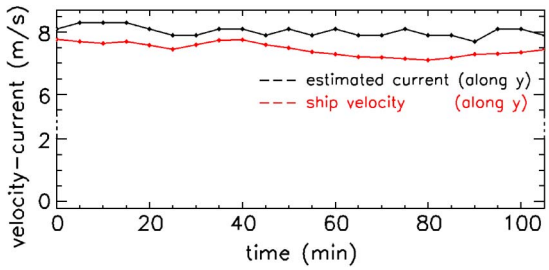

Fig. 6. Comparison between (black) the estimated current component U_y along the ship motion and (red) the ship velocities measured by GPS.

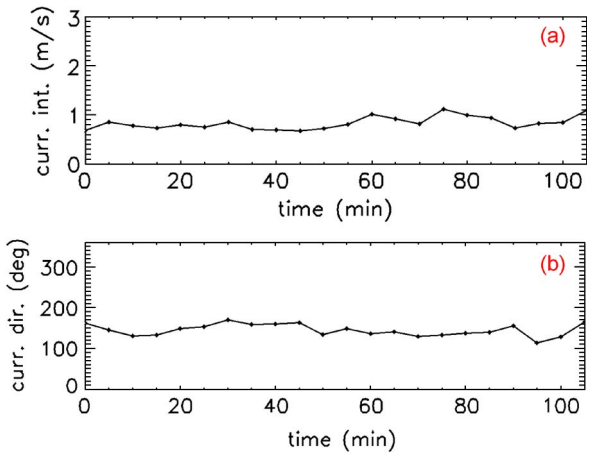

Fig. 7. Estimated current obtained after the removal of the true ship velocities. (a) Intensity U. (b) Direction with respect to north.

agreement, even considering that measurements have been recorded in open sea conditions, where, typically, the surface currents are less than 1 m/s.

A rough estimation of the surface currents U_{sc} in the surveyed area can be done using the approach proposed by Faltinsen [13]. Here, several components were identified, of which mainly two are of interest in our geographical area: the component induced by the sea circulation (U_m) and that one generated by the local wind (U_w). The former, by using the simulated data at a depth of 5 m, freely available from the Italian Ministry for the Environment and Territory (http://gnoo.bo.ingv.it/mfs/ analysis_archive.htm), can be estimated in 0.4 m/s. The latter can be predicted by using the first approximation proposed in [13], i.e., $U_w(\text{at sea level}) = 0.02\ U_{10}$, being U_{10} the wind velocity measured 10 m above the sea level. A value of U_{10} varying between 25 and 30 knots (with a mean direction of 135° from N, i.e., about 210° from the ship direction) was measured by the anemometer of the ship during the trials. Surface currents U_{sc} of 0.25–0.3 m/s and 0.65–0.7 m/s can be then predicted for U_w and $U_m + U_w$, respectively, i.e., the latter very close to the prediction of the NSP model (see Fig. 7). As pointed out also by Fig. 8, showing (black arrow) the trajectory of the ship and (red arrow) the direction of the current, the direction is constant and coincides with the one provided by the model for the sea circulation and the local wind in the surveyed zone [14]–[16].

VI. Conclusion

This letter has dealt with the problem of the sea state prediction starting from marine radar collected on a moving ship.

Fig. 8. Pictorial view of (black lines) the positions of the ship and (red lines) the current direction.

In this framework, the estimate of surface current plays a key role in the inversion procedure because it affects the filtering necessary to cut off all the undesired phenomena and noise on the data. In this letter, we have proposed a method for the estimation of the ocean surface current that is based on the "correlation" between the measured spectrum and the characteristic function having the dispersion relation as a support. First, the proposed technique has been validated through a comparison with the synthetic data coming from a numerical wave tank, and a comparison with the classical LS procedure has been also performed. After that, a comparison with the experimental data recorded during an *ad hoc* full-scale trial on a moving ship in waves has been considered.

REFERENCES

[1] R. Young, W. Rosenthal, and F. Ziemer, "Three-dimensional analysis of marine radar images for the determination of ocean wave directionality and surface currents," *J. Geophys. Res.*, vol. 90, no. C1, pp. 1049–1059, 1985.

[2] F. Ziemer and W. Rosenthal, "Directional spectra from shipboard navigation radar during LEWEX," in *Directional Ocean Wave Spectra: Measuring, Modeling, Predicting, and Applying*, R. C. Beal, Ed. Baltimore, MD: The Johns Hopkins Univ. Press, 1991, pp. 125–127.

[3] J. C. Nieto Borge, R. G. Rodriguez, K. Hessner, and I. P. Gonzales, "Inversion of marine radar images for surface wave analysis," *J. Atmos. Ocean. Technol.*, vol. 21, no. 8, pp. 1291–1300, Aug. 2004.

[4] J. C. Nieto Borge and C. Guedes Soares, "Analysis of directional wave fields using X-band navigation radar," *Coast. Eng.*, vol. 40, no. 4, pp. 375–391, Jul. 2000.

[5] J. C. Nieto Borge, "Analisis de Campos de Oleaje mediante radar de navegacion en banda X-," Ph.D. dissertation, Univ. Madrid, Madrid, Spain, 1997.

[6] K. Hessner, K. Reichert, J. Dittmer, J. C. Nieto Borge, and H. Gunther, "Evaluation of WaMoS II wave data," in *Proc. 4th Int. Symp. Ocean Wave Meas. Anal.*, San Francisco, CA, 2000, pp. 221–230.

[7] P. H. Y Lee, J. D. Barter, K. L. Beach, C. L. Hindman, B. M. Lade, H. Rungaldier, J. C. Shelton, A. B. Williams, R. Yee, and H. C. Yuen, "X band microwave backscattering from ocean waves," *J. Geophys. Res.*, vol. 100, no. C2, pp. 2591–2611, 1995.

[8] W. J. Plant and W. C. Keller, "Evidence of Bragg scattering in microwave Doppler spectra of sea return," *J. Geophys. Res.*, vol. 95, no. C9, pp. 16 299–16 310, 1990.

[9] L. B. Wenzel, "Electromagnetic scattering from the sea at low grazing angles," in *Surface Waves and Fluxes*, G. L. Geernaert and W. J. Plant, Eds. Norwell, MA: Kluwer, 1990, pp. 41–108.

[10] C. M. Senet, J. Seemann, S. Flampouris, and F. Ziemer, "Determination of bathymetric and current maps by the method DiSC based on the analysis of nautical X-band radar image sequences of the sea surface (November 2007)," *IEEE Trans. Geosci. Remote Sens.*, vol. 46, no. 8, pp. 2267–2279, Aug. 2008.

[11] C. Lugni, "An investigation on the interaction between free-surface waves and a marine structure," Ph.D. dissertation, Univ. Rome 'La Sapienza, Rome, Italy, 1999.

[12] P. Wang, Y. Yao, and M. P. Tulin, "An efficient numerical wave tank for non-linear water waves, based on the multi-subdomain approach with BEM," *Int. J. Numer. Methods Fluids*, vol. 20, no. 12, pp. 1315–1336, 1995.

[13] O. M. Faltinsen, *Sea Loads on Ships and Offshore Structures*. Cambridge, U.K.: Cambridge Univ. Press, 1993.

[14] P. F. J Lermusiaux and A. R. Robinson, "Features of dominant mesoscale variability, circulation patterns and dynamics in the Strait of Sicily," *Deep-Sea Res., Part I*, vol. 48, no. 9, pp. 1953–1997, Aug. 1997.

[15] K. Beranger, L. Mortier, and M. Crepon, "Seasonal variability of water transport through the Straits of Gibraltar, Sicily and Corsica, derived from a resolution model of the Mediterranean circulation," *Prog. Oceanogr.*, vol. 66, no. 2–4, pp. 341–364, Aug.–Sep. 2005.

[16] R. Sorgente, A. F. Drago, and A. Ribotti, "Seasonal variability in the Central Mediterranean Sea circulation," *Annal. Geophysi.*, vol. 21, pp. 299–322, 2003.